Melanocyte-secreted fibromodulin promotes an angiogenic microenvironment

Irit Adini,[1] Kaustabh Ghosh,[2] Avner Adini,[1] Zai-Long Chi,[1] Takeru Yoshimura,[1] Ofra Benny,[1] Kip M. Connor,[3] Michael S. Rogers,[1] Lauren Bazinet,[1] Amy E. Birsner,[1] Diane R. Bielenberg,[1] and Robert J. D'Amato[1,4]

[1]Vascular Biology Program, Department of Surgery, Boston Children's Hospital, Harvard Medical School, Boston, Massachusetts, USA. [2]Department of Bioengineering, University of California, Riverside, California, USA. [3]Angiogenesis Laboratory, Department of Ophthalmology, Harvard Medical School, Massachusetts Eye and Ear Infirmary, Boston, Massachusetts, USA. [4]Department of Ophthalmology, Harvard Medical School, Boston, Massachusetts, USA.

Studies have established that pigmentation can provide strong, protective effects against certain human diseases. For example, angiogenesis-dependent diseases such as wet age-related macular degeneration and infantile hemangioma are more common in light-skinned individuals of mixed European descent than in African-Americans. Here we found that melanocytes from light-skinned humans and albino mice secrete high levels of fibromodulin (FMOD), which we determined to be a potent angiogenic factor. FMOD treatment stimulated angiogenesis in numerous in vivo systems, including laser-induced choroidal neovascularization, growth factor–induced corneal neovascularization, wound healing, and Matrigel plug assays. Additionally, FMOD enhanced vascular sprouting during normal retinal development. Deletion of *Fmod* in albino mice resulted in a marked reduction in the amount of neovascularization induced by retinal vein occlusion, corneal growth factor pellets, and Matrigel plugs. Our data implicate the melanocyte-secreted factor FMOD as a key regulator of angiogenesis and suggest an underlying mechanism for epidemiological differences between light-skinned individuals of mixed European descent and African-Americans. Furthermore, inhibition of FMOD in humans has potential as a therapeutic strategy for treating angiogenesis-dependent diseases.

Introduction

Age-related macular degeneration (AMD) is the leading cause of vision loss among the elderly in developed countries. The advanced form of the disease is characterized by abnormal blood vessel growth and formation of a choroidal neovascular (CNV) membrane under the macula. Population-based epidemiological studies by Vanderbeek in 2011 compared the incidence of exudative AMD among different races in 113,234 individuals. For baseline reference, African-Americans have the most melanin, Asians have an intermediate level, and light-skinned individuals of mixed European descent have the lowest. Relative to what is found in light-skinned individuals of mixed European descent, exudative AMD is 55% less frequent in African-Americans and 46% less frequent in Asian-Americans. These findings support the hypothesis that lower pigmentation is a risk factor for neovascular AMD (1–3). Studies examining the correlation between race, ethnicity, and incidence of uveal melanoma indicate an influence of iris color on the disease. The frequency of uveal melanoma is highest in light-skinned individuals of mixed European descent, followed by Hispanics, Asians, and African-Americans, with an 18:1 ratio of incidence between light-skinned individuals of mixed European descent and African-Americans (4–6). Similar to the trend of occurrence seen with wet AMD, cutaneous melanoma and infantile hemangioma are much more prevalent in light-skinned individuals of mixed European descent than African-Americans. These facts suggest that low levels of melanin correlate with the development of angiogenic ocular and skin diseases. Since intracellular pigment levels of retinal pigment epithelium (RPE) cells do not differ greatly among races, our studies focused on melanocytes, the main source of ocular pigment.

Functionally, melanin surrounds the nucleus of a cell to protect DNA from the harmful effects of UV radiation (7). In the eye, pigment is limited to the uveal tract, consisting of the iris, ciliary body, and choroid, where it protects against UV-induced damage (8). Melanogenesis is the cellular process of pigment production that occurs in melanosomes. These specialized organelles are surrounded by a lipid membrane within the melanocyte, one of the few cell types that can synthesize melanin. In the skin, melanocytes can distribute melanin-containing melanosomes to surrounding cells such as keratinocytes. The process of melanogenesis is stimulated by several effectors including UV irradiation, melanocyte-stimulating hormone (α-MSH), and FGF2 (7, 9–12). The melanin biosynthesis pathway is initiated with tyrosinase-mediated conversion of the amino acid tyrosine to dopaquinone. The pathway is also dependent on 2 related enzymes, tyrosinase-related protein-1 (TRP-1), which results in the production of black rather than brown melanin, and TRP-2, which acts as a dopachrome tautomerase, isomerizing the melanogenic intermediate *L*-dopachrome to 5,6-dihydroxyindole-2-carboxylic acid (DHICA) in the biosynthesis of melanin. *L*-dopachrome will also spontaneously decarboxylate to form 5,6-dihydroxyindole (DHI), a second melanin precursor (13). As a key enzyme in pigment synthesis, mutations in the tyrosinase gene led to catalytically inactive enzyme or a complete lack of the protein. This can result in the absence of melanin, producing a condition known as albinism (13–17).

Local regulation of angiogenesis is dependent on the balance between endogenous inhibitors and stimulators. This balance is determined by genetic factors inherited as quantitative traits in a variety of in vivo angiogenesis models (18). Based on these findings and the human epidemiological data linking lighter skin color with angiogenic diseases, we investigated whether melano-

Conflict of interest: The authors have declared that no conflict of interest exists.
Citation for this article: *J Clin Invest.* 2014;124(1):425–436. doi:10.1172/JCI69404.

cytes have a role in regulating angiogenesis in pigmented tissues. To test this hypothesis, we examined angiogenesis in numerous models using pigmented (C57BL) or albino C57BL/6J (C57) mice.

Results

Effects of pigmentation on angiogenesis. To determine the effect of pigmentation on angiogenesis, we performed the corneal neovascularization assay in 2 strains of mice that are genetically identical except for expression of the tyrosinase gene. We implanted FGF2 pellets (80 ng) into corneal micropockets of WT C57 (C57BL expressing normal tyrosinase) and mutant B6(Cg)-*Tyr*$^{c\text{-}2J}$/J mice (C57-albinos, which have a G→T at nucleotide 291 in the tyrosinase gene, nullifying expression) and examined blood vessel growth in the cornea (which does not contain melanocytes) and the underlying iris (which contains melanocytes) 5 days after pellet implantation (Figure 1, A and B). Upon gross examination, we observed that neovascularization in the cornea appeared similar in both the C57-albino and C57BL mice (Figure 1A). However, the C57-albino mice developed iris neovascularization with hyphemas (blood in the anterior chamber) with much higher frequency than the C57BL mice (Figure 1A). In order to compare neovascularization of the iris, where vessel growth has been stimulated by the FGF2 in the corneal pellet, we injected both strains intravenously with FITC-conjugated BS-1 lectin to label perfused blood vessels. We observed aggressive neovascularization in the C57-albino iris (Figure 1B) to a 9-fold greater extent than in C57BL mice, as measured by increased fluorescent iris vessel area (VA) 5 days after pellet implantation (Figure 1C). Additionally, we performed analysis of vWF, a constitutive endothelial cell protein, as a marker of endothelial cells in the iris. Western blot analysis revealed more vWF in protein lysates from nonpigmented (C57-albino) irises after FGF2 stimulation, validating the observation that FGF2 pellets in nonpigmented mice induced more new blood vessel growth (Supplemental Figure 1; supplemental material available online with this article; doi:10.1172/JCI69404DS1).

To determine whether these findings were ocular specific, we investigated angiogenesis in pigmented versus albino murine skin. We began by measuring baseline cutaneous vessel density, as visualized by CD31 immunofluorescent staining, and observed no significant difference (Figure 1D). We then sought to determine whether wound angiogenesis was differentially affected by skin pigmentation. To that end, we created a 1-mm full-thickness punch biopsy wound in the ears of each strain and measured subsequent vessel formation into the wound edge. Since these new vessels provide a conduit for nutrients and other mediators, their ingrowth is an essential feature of wound repair. Five days after wounding, we injected mice intravenously with FITC-conjugated dextran to visualize perfused blood vessels (Figure 1E). Consistent with our results in the iris, we observed that mean fluorescent vascular area around the wound was 2.5-fold greater in C57-albino mice than in C57BL mice (Figure 1F).

To study the molecular mechanism responsible for the observed differences in angiogenesis between C57-albino and C57BL mice, we utilized an in vitro coculture system. It has been demonstrated that the ability of capillary endothelial cells to migrate and form tubes is essential for new sprout formation (19). Thus, we examined the migratory capacity of human dermal microvascular endothelial cells (HMVEC) in response to conditioned medium (CM) from immortalized, amelanotic melanocytes isolated from Balb/c albino mice. Balb/c melanocytes express enzymatically-inactive tyrosinase due to a homozygous point mutation (T<u>G</u>T→T<u>C</u>T) in the tyrosinase gene resulting in a lack of melanin (20). So that they would serve as a control cell line, pigmentation was restored in these cells by correcting the point mutation using an RNA-DNA oligonucleotide (gift from Alexeev Y. Vitali; Thomas Jefferson University, Philadelphia, Pennsylvania, USA) (Supplemental Figure 2).

Analysis of HMVEC migration revealed no significant difference upon exposure to control (unconditioned) medium and CM from pigmented melanocytes (average of 32 cells migrated per 100 μm^2 field for both) (Figure 1G). However, migration of HMVECs toward CM from nonpigmented melanocytes was 50% higher than control (an average 50 cells/field versus 32) (Figure 1G). These data suggest that nonpigmented melanocytes secrete a stimulator of HMVEC migration, rather than pigmented melanocytes secreting an inhibitory factor. To further elucidate this finding, pigmented melanocytes were grown in medium lacking tyrosine, thereby arresting new melanin synthesis. CM from these cells was found to stimulate HMVEC migration 50% over control, a promigratory effect mimicking that of nonpigmented melanocytes (Figure 1H). Similar results were observed with CM from cultured, primary human melanocytes isolated from the epidermis of light-skinned individuals of mixed European descent or African-Americans. Specifically, CM from melanocytes from light-skinned individuals of mixed European descent increased migration of HMVECs 1.5-fold compared with CM from the more highly pigmented African-American melanocytes (Figure 1I). Collectively, these findings indicate that melanocytes can secrete a stimulator of EC migration. We then sought to determine whether the CM from pigmented and nonpigmented melanocytes also differentially influenced endothelial cell survival and/or proliferation. As such, we performed cell proliferation assays with HMVECs in the presence and absence of CM from pigmented and nonpigmented human and murine melanocytes. We exposed HMVECs to respective CMs for 2 days, after which cell viability was evaluated using WST-1 reagent. We observed that CM from nonpigmented murine melanocytes promoted HMVEC viability and proliferation more than that of pigmented murine melanocytes (Figure 1J). Additionally, human melanocytes from light-skinned individuals of mixed European descent stimulated HMVEC proliferation to a greater extent than African-American melanocytes (Figure 1K). Taken together, our data suggest that low-pigmented melanocytes secrete a stimulator of endothelial cells.

Nonpigmented melanocytes secrete fibromodulin. To investigate the molecular mechanism responsible for stimulation of angiogenesis by amelanotic melanocytes, we performed microarray-based gene expression analysis of pigmented and nonpigmented melanocytes (see Methods). For this analysis, we employed a candidate gene approach in which candidates were selected using the following criteria: first, mRNA showing greater than 10-fold increased expression by nonpigmented over pigmented melanocytes was selected. Of these, candidates were selected if their encoded proteins were (a) known to be secreted, (b) had high homology between mouse and human, and (c) were previously implicated in either angiogenesis or AMD. An intriguing candidate which emerged from these criteria was fibromodulin (FMOD). FMOD is a 42-kDa secreted protein belonging to the leucine-rich repeat protein family of proteoglycans that interacts with collagen types I and II (21–23) and is known to contribute to inflammatory path-

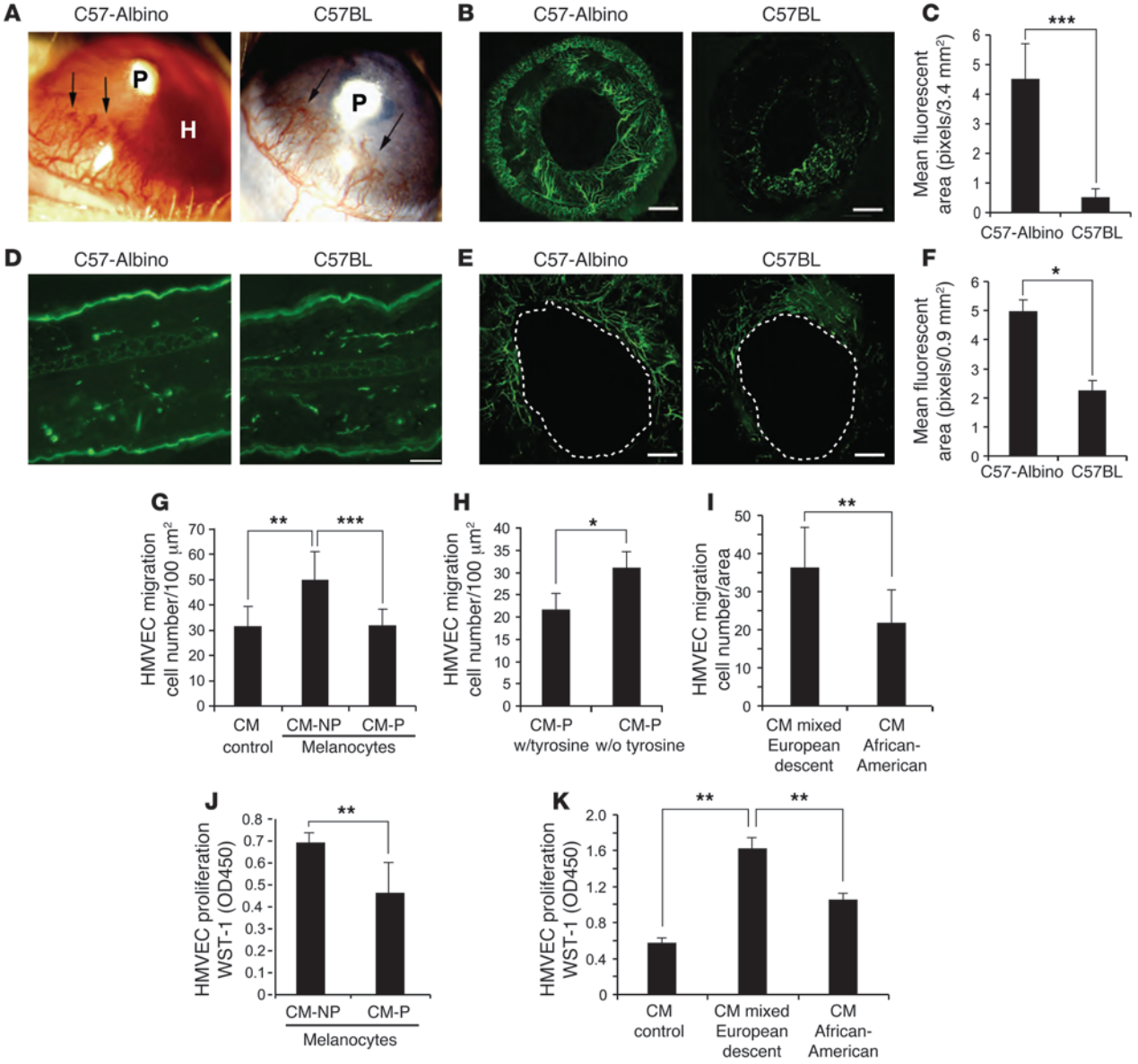

Figure 1

Effect of pigmented and nonpigmented melanocytes on angiogenesis. (**A**) Corneal neovascular response in different inbred mouse strains induced by corneal implantation of FGF2 pellets (P) in C57-albino mice (left) with hyphema formation (H) and C57BL mice (right). The experiment included 10 eyes per group. (**B**) Iris neovascularization visualized with FITC–BS-1 lectin. Scale bars: 500 μm. The experiment included 10 eyes per group. (**C**) Quantification of iris vessel density of C57-albino versus C57BL. Experiment included 10 eyes per group. (**D**) Normal skin vessel density in C57-albino and C57BL mice labeled with CD31 antibody. Scale bar: 20 μm. (**E**) Angiogenesis during wound healing in ear skin. Blood vessels were perfused with FITC-conjugated BS-1 lectin (green) and photographed. Scale bars: 10 μm. The experiment included 5 wounds per group. (**F**) Analysis of microvessel density in albino ear skin. (**G**) Migration of HMVECs to CM from albino (CM-NP) and pigmented (CM-P) melanocytes. (**H**) Migration of HMVECs to CM from pigmented melanocytes grown in the presence and absence of tyrosine. (**I**) Migration of HMVECs to CM from human melanocytes (mixed European descent and African-American) through Transwells. (**J**) HMVEC proliferation in response to CM from nonpigmented or pigmented melanocytes for 24 hours; analysis by WST-1 at 450 O.D. (**K**) HMVECs incubated with CM from human melanocytes (mixed European descent and African-American) for 24 hours, followed by proliferation analysis with WST-1 at 450 O.D. All experiments were repeated at least 3 times. *$P < 0.01$; **$P < 0.001$; ***$P < 0.0001$.

ways (24). FMOD protein localizes to the cytosol and contains a secretory sequence (25–31). While at present there are no reports directly linking FMOD to AMD, it is known that a major point of susceptibility for the development of AMD is complement factor H (CFH), an immune regulator that inhibits complement activation (32). Poor binding of CFH to FMOD frees CFH to bind C1q, leading to complement activation and resulting pathological processes. Thus, we investigated whether FMOD may be one of the proteins responsible for the pigment-mediated difference in angiogenic diseases of tissue-containing melanocytes.

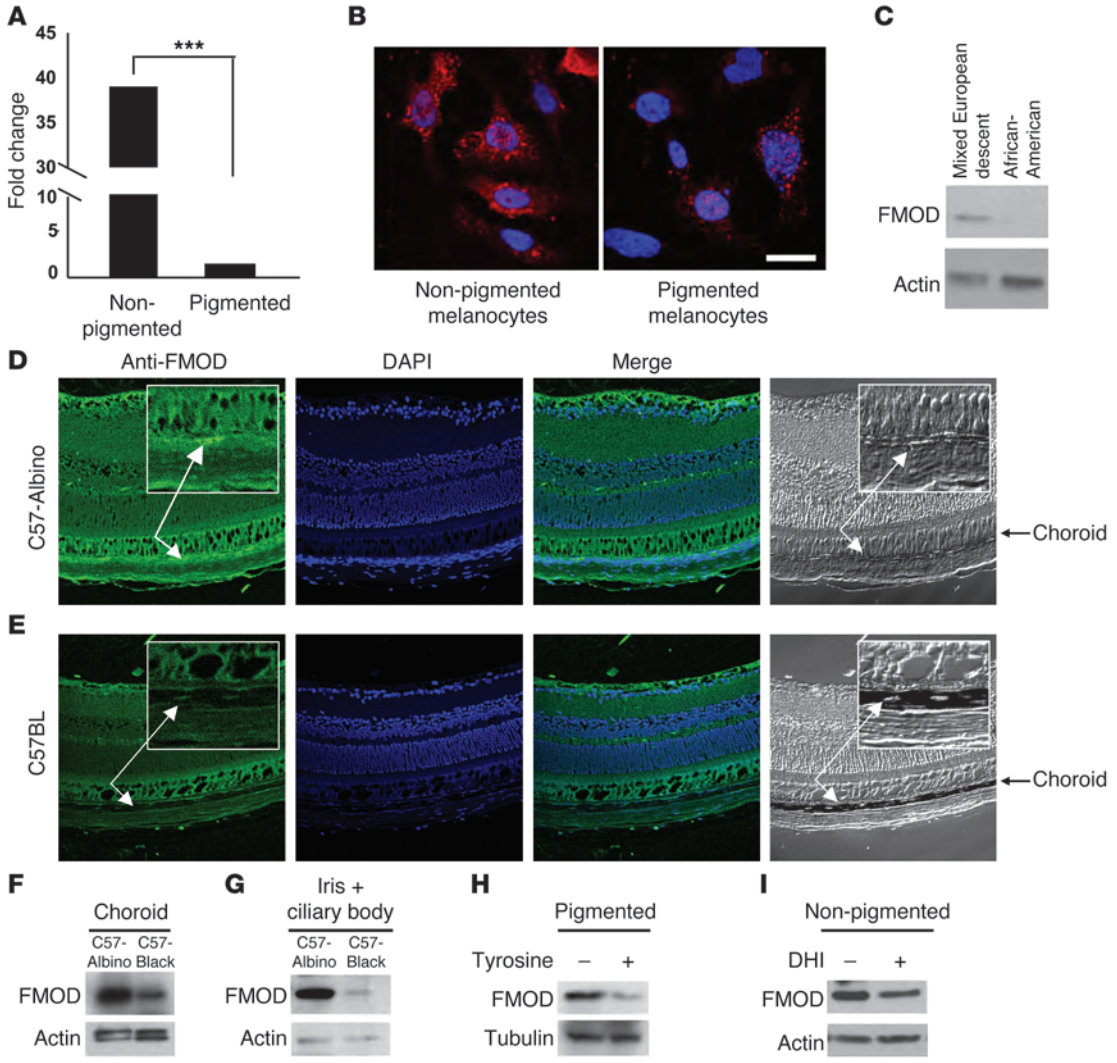

Figure 2

FMOD expression in pigmented and nonpigmented melanocytes. (**A**) *FMOD* mRNA in nonpigmented (albino) and pigmented mouse melanocytes was measured by qRT-PCR and normalized to the level of GAPDH; ***$P < 0.0001$. (**B**) Nonpigmented (albino, left) and pigmented (right) melanocytes were stained with FMOD and anti-mouse TRITC antibody and visualized by fluorescence microscopy. Nuclei were counterstained with DAPI. Scale bar: 200 μm. (**C**) CM from melanocytes from African-Americans and light-skinned individuals of mixed European descent were assessed by Western blot using an antibody against FMOD. (**D**) Retinal sections from C57-albino and (**E**) C57BL mice were stained for FMOD and visualized by confocal microscopy. Nuclei were counterstained with DAPI. Arrows show the choroid layer. Original magnification, ×40. (**F** and **G**) FMOD protein was examined by Western blot in choroid melanocytes (**F**) and iris (**G**) from C57BL and C57-albino mice. Each group had a minimum of 5 mice. $n \geq 10$. β-Actin was used as a loading control. (**H**) FMOD protein from pigmented cells grown in the presence and absence of tyrosine-free medium was analyzed by Western blot. β-Actin was used as a loading control. (**I**) FMOD protein from nonpigmented cells treated with DHI was analyzed by Western blot. β-Actin was used as a loading control.

Initial cell culture experiments verified that nonpigmented melanocytes have high expression levels of FMOD, whereas pigmented melanocytes express low levels (shown in Figure 2C). Given this, we sought to examine variances in gene expression of *FMOD* mRNA between pigmented and nonpigmented cells using real-time RT-PCR analysis and immunofluorescent staining. We found that nonpigmented mouse melanocytes express dramatically more (40-fold) *FMOD* mRNA than pigmented melanocytes (Figure 2A). Immunohistochemical staining further confirmed this observation (Figure 2B, red color). Consistently, Western blot analysis revealed that CM from human melanocytes isolated from light-skinned individuals of mixed European descent contained higher levels of FMOD protein than melanocytes of African-Americans (Figure 2C).

To investigate the localization of *FMOD* in ocular tissue, we performed immunofluorescent staining for FMOD on cryosections from C57-albino and C57BL mouse retinas. Strong FMOD staining was seen in the nonpigmented choroids of C57-albino mice (Figure 2D), but not in the heavily pigmented choroids of C57BL mice (Figure 2E). To confirm that the presence of melanin in the tissue of WT mice did not simply mask the fluorescent staining, FMOD levels were also assessed by Western blot analysis in iso-

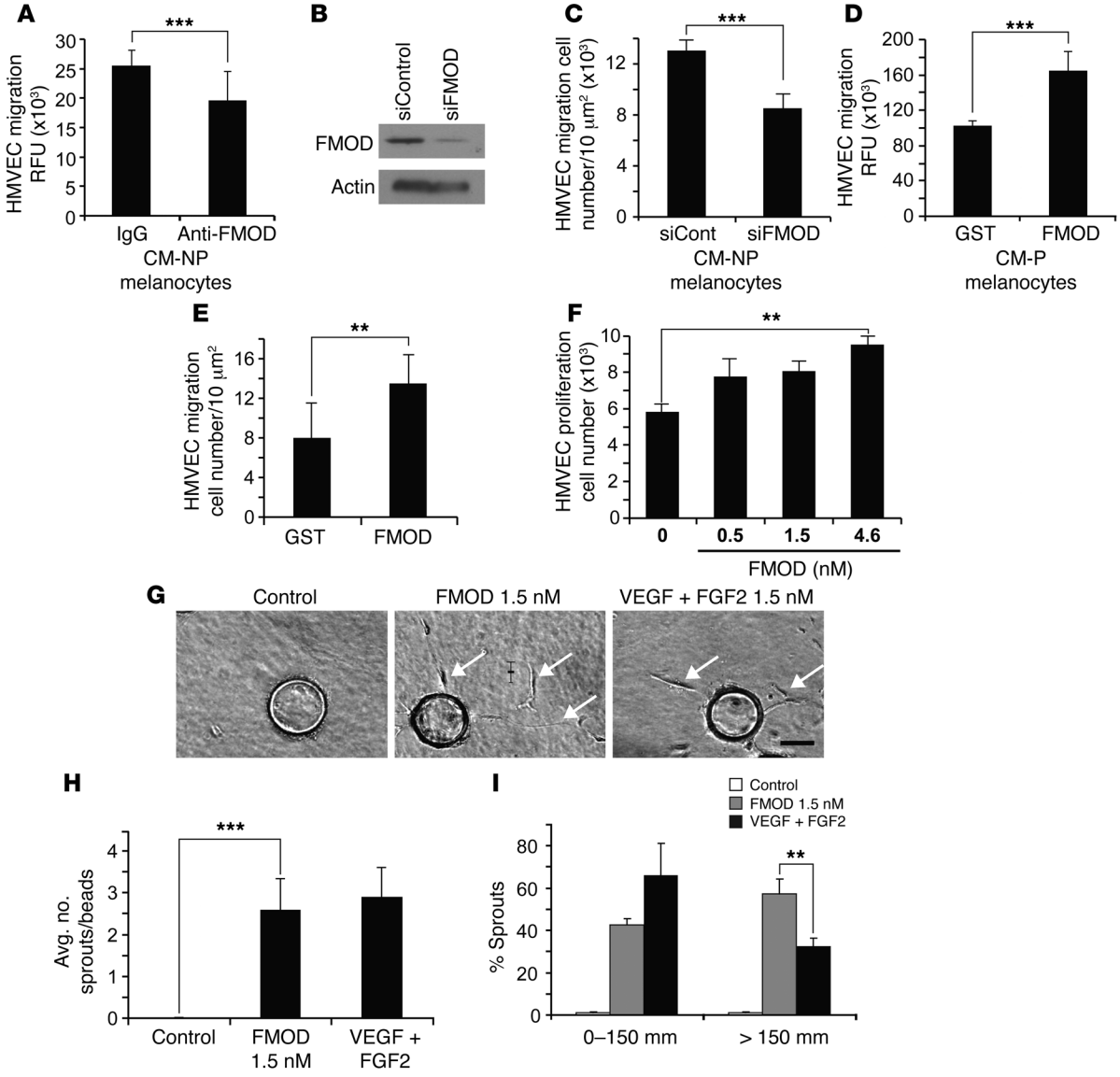

Figure 3

FMOD-induced migration, proliferation and sprouting of HMVECs. (**A**) HMVEC migration in response to FMOD-neutralized CM from nonpigmented melanocytes, IgG was used as a control. (**B**) siRNA-mediated knockdown of FMOD was confirmed by Western blot. β-Actin was used as a loading control. (**C**) HMVEC migration in response to CM from nonpigmented melanocytes transfected with FMOD-specific siRNA. (**D**) HMVEC migration was assessed in CM from pigmented melanocytes containing 2 μM recombinant FMOD or GST. (**E**) HMVEC migration with recombinant FMOD or control-GST. (**F**) Proliferation of HMVECs with designated concentrations of FMOD was assessed by cell counting. (**G**) HMVECs are coated onto beads and embedded into a fibrin gel in the presence of medium alone, medium plus 1.5 nM FMOD, or medium plus VEGF-A/FGF2 (1.5 nM each). Arrows show sprouts. Scale bar: 100 μm. (**H**) Average number of sprouts per bead was not significantly different between 1.5 nM FMOD and positive VEGF-A/FGF2 control. Significant differences were observed between recombinant FMOD and control. (**I**) Percentage of sprouts with a length less than 150 μm in the presence of 1.5 nM FMOD and 1.5 nM VEGF-A+FGF2 versus those with length greater than 150 μm in the presence of FMOD or 1.5 nM VEGF-A/FGF2. 1.5 nM FMOD increased cell migration over VEGF-A/FGF2. $^{**}P < 0.001$; $^{***}P < 0.0001$.

lated choroids (Figure 2F), irises, and ciliary bodies (Figure 2G). As predicted, C57-albinos consistently expressed higher levels of FMOD throughout the ocular tissue than WT C57BL mice.

Our next aim was to examine whether tyrosinase itself, or a soluble melanin intermediate, was responsible for the regulation of FMOD expression in pigmented tissue. To elucidate this, we examined normal, pigmented melanocytes cultured in medium lacking tyrosine. In the absence of tyrosine, cells do not actively produce new intermediate melanin products nor new melanin (brown black polymer). Resultant FMOD expression was then analyzed by Western blot (Figure 2H); similar results were shown in CM from pigmented cells (Supplemental Figure 3). Our findings revealed that, despite the presence of preexisting melanin inside the cells, removal of tyrosine from the medium resulted in increased FMOD expression at a level consistent with that seen in nonpigmented cells. This indicates that it is not the final insoluble end product of melanin polymer,

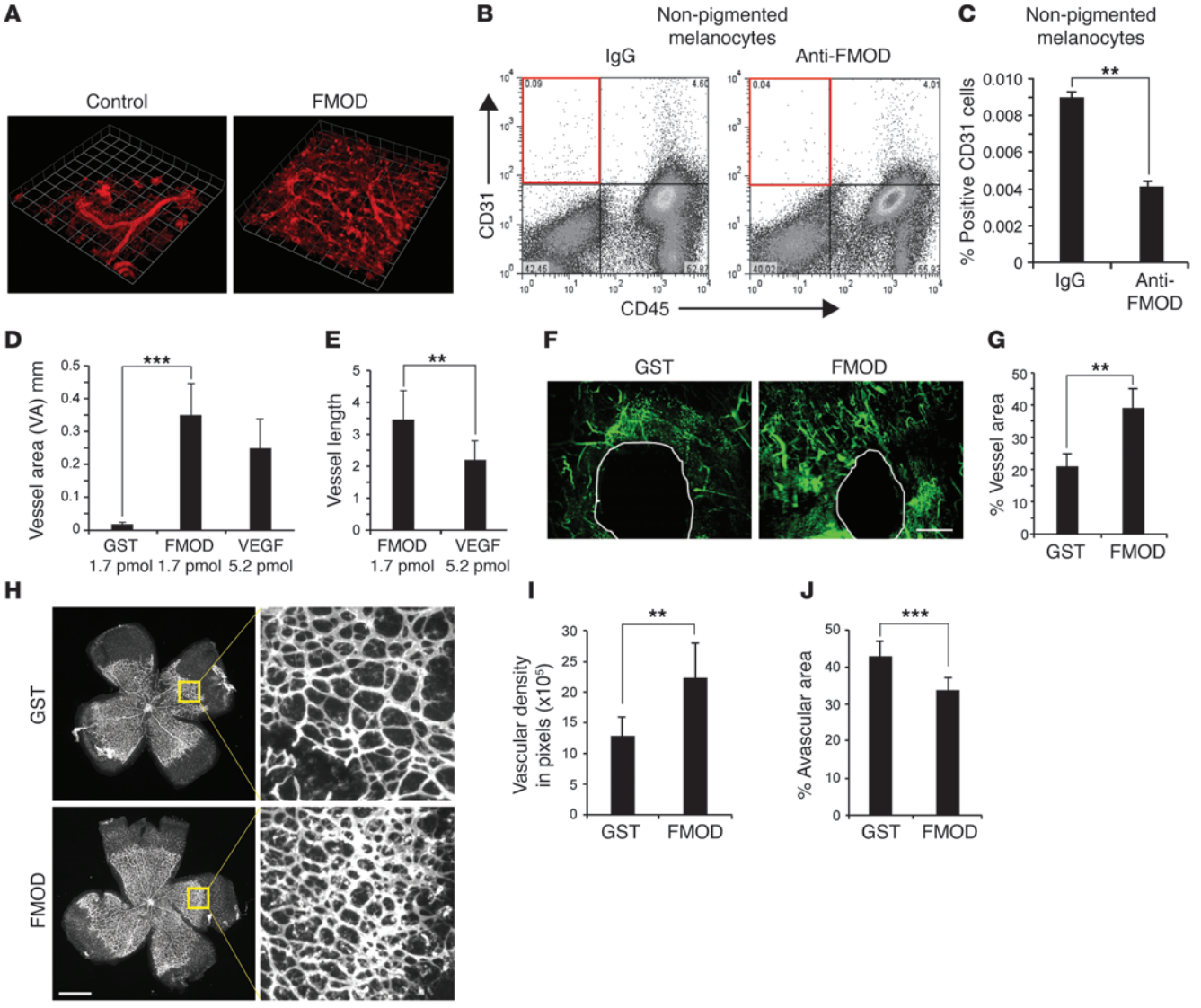

Figure 4

FMOD induces endothelial cell migration in vivo. (**A**) HVMECs combined with BM-MSC (10:1) with or without recombinant h-FMOD were mixed with Matrigel. Perfused vessels were labeled with human-specific rhodamine-labeled lectin and visualized with confocal microscopy; $n = 6$ plugs per group; experiment repeated 3 times. Original magnification, ×5. (**B** and **C**) Migration of host endothelial cells into Matrigel plugs containing nonpigmented melanocytes neutralized by anti FMOD or IgG as a control. Cells were stained for CD31 and CD45 and analyzed by FACS; $n = 10$ per group (**C**). (**D**) The corneal micropocket assay was performed with pellets containing 1.69 μM of FMOD, 1.69 μM GST, or 5.2 μM VEGF-A. FMOD versus control was significantly different. No significant difference in VA was found between FMOD and VEGF-A. The experiment was repeated 3 times and included 10 eyes per group in each experiment. (**E**) FMOD stimulated longer vessels than VEGF-A. (**F**) FMOD (2 μM) promotes angiogenesis in wound healing in ear skin of C57BL/6J mice; blood vessels visualized by FITC-conjugated dextran (green). Scale bar: 500 μm. (**G**) Quantification of blood vessel density; $n = 5$ mice per group; 2 punches per mouse. (**H**) Recombinant FMOD (1.19 μM) or control-GST injected into the vitreous of 4-day-old pups; $n = 5$ mice per group. On day 7, retinas were dissected and labeled (Alexa Fluor 594–conjugated isolectin). Scale bar: 1 nm. Original magnification, ×5. (**I**) Neovascular density was assessed by quantifying the capillary junctions within 4 equal areas (ImageJ). (**J**) Avascular retina was calculated as percentage of total retinal area quantified (ImageJ); $n = 9$ in each group, experiment was repeated twice. $^{**}P < 0.001$; $^{***}P < 0.0001$.

but rather an earlier intermediate factor produced in the process of functional melanogenesis, that has direct effects on FMOD production. As a further step, we screened the known soluble melanin intermediates for effects on FMOD expression. Nonpigmented cells were cultured in medium lacking tyrosine to which we added individual soluble melanin intermediary products such as DHI. DHI is essential for melanin formation via tyrosinase by catalyzed oxidation of tyrosine (33). Albino melanocytes supplemented with DHI produced a reduced level of FMOD compared with nonsupplemented cells (Figure 2I), showing that intermediates of the melanogenesis process influence cellular expression of FMOD.

FMOD stimulates endothelial cell functions in vitro. To show that a substantial component of the stimulatory effects of albino CM on HMVEC migration and proliferation was due to FMOD expres-

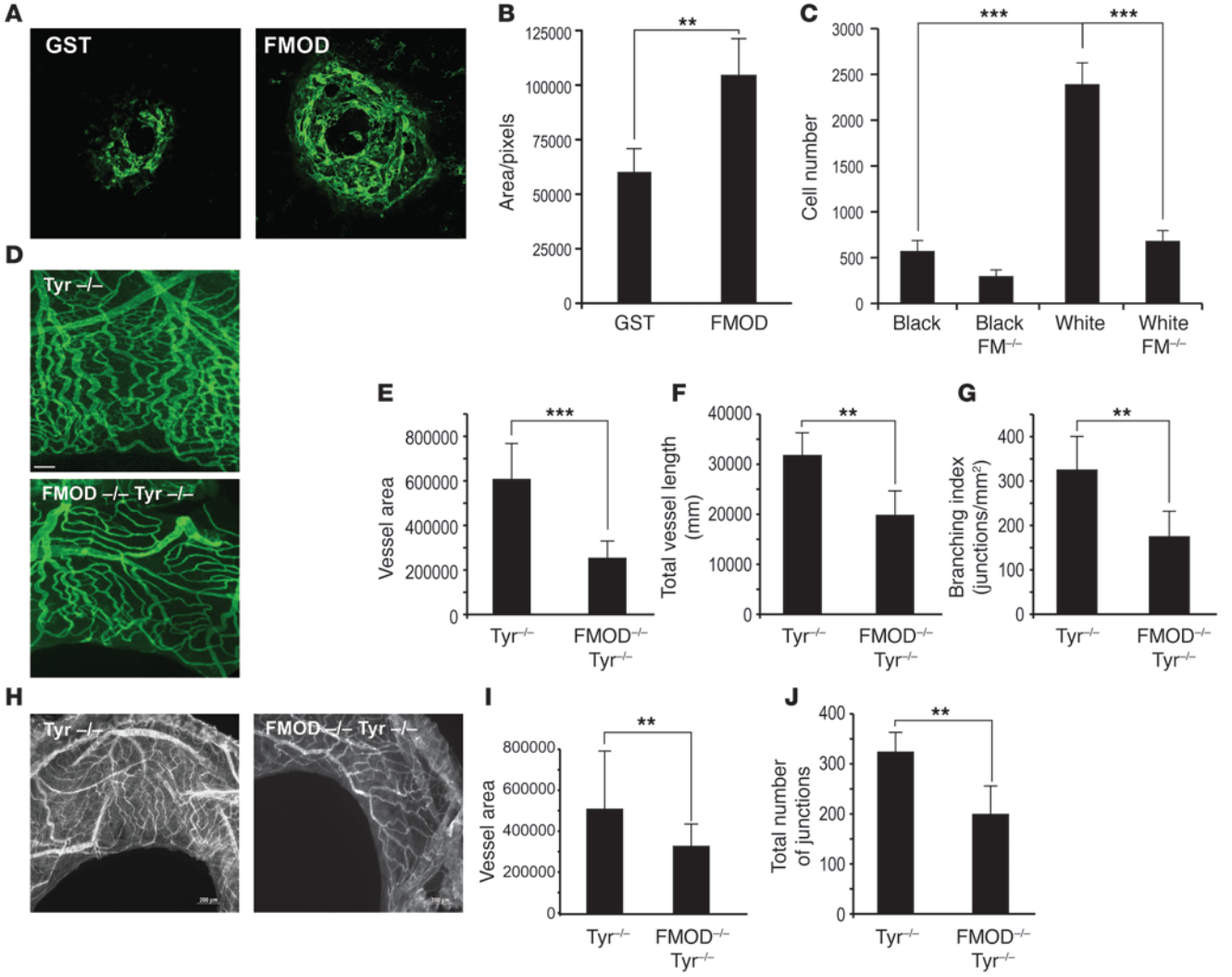

Figure 5

FMOD enhances CNV formation and induces endothelial cell migration in vivo. (**A**) CNV lesions were induced by subretinal laser burns around the optic disc. After laser treatment, intravitreal injection of 35 ng/0.5 μl/eye rh-FMOD or control-GST was performed. Representative images of CNV lesions stained with lectin-FITC are shown. Original magnification, ×10. (**B**) Data are presented as mean pixel number ± SEM. *t* test. $n = 30–40$. (**C**) To quantify the effect of *Fmod*-KO (*Fmod*$^{-/-}$ in C57-albino compared with *Fmod*$^{+/+}$ C57-albino) on migration of host endothelial cells into Matrigel plugs containing 500 ng/ml FGF-2, cells were stained for CD31 and CD45 and analyzed by FACS. $n = 10$. Each experiment was repeated 3 times. (**D**) Iris neovascularization after FGF2 corneal pellet implantation was visualized with FITC–BS-1 lectin. Scale bar: 500 μm. (**E**) Quantification of iris VA of C57-albino versus *Fmod*$^{-/-}$ albino. (**F**) Quantification of total iris vessel length of C57-albino versus *Fmod*$^{-/-}$ albino. (**G**) Quantification of iris branching index of C57-albino versus *Fmod*$^{-/-}$ albino. (**H**) RVO lesions were induced by laser burns around the optic nerve. After laser treatment, images of iris neovascularization stained with lectin-GSII were analyzed. (**I**) Quantification of iris VA of C57-albino versus *Fmod*$^{-/-}$ albino. (**J**) Quantification of total iris vessel length of C57-albino versus *Fmod*$^{-/-}$ albino. $^{**}P < 0.001$; $^{***}P < 0.0001$.

sion, we next neutralized FMOD. Inhibiting FMOD in the CM via neutralizing antibody resulted in reduced HMVEC migration as compared with control IgG–treated CM (Figure 3A). Additionally, siRNA was used to knock down FMOD expression in nonpigmented murine melanocytes and silencing was confirmed by Western blot (Figure 3B). In a coculture experiment, we observed that siRNA-mediated silencing of FMOD in the melanocytes resulted in 35% reduction of HMVEC migration (Figure 3C). We found that CM from pigmented melanocytes was unable to stimulate migration and proliferation of endothelial cells. To determine whether this inability was due to the low expression of FMOD, exogenous FMOD was added to the CM. Supplementation of FMOD into CM from pigmented melanocytes increased HMVEC migration by 2-fold in comparison with control (Figure 3D). Indeed, recombinant FMOD protein alone stimulated HMVEC migration and proliferation in a dose-dependent fashion (Figure 3, E and F, respectively).

To investigate FMOD's ability to promote angiogenesis, a multistage process that involves endothelial cell growth, motility, and extracellular matrix degradation, we performed a 3D in vitro sprouting angiogenesis assay (34, 35). Examination of HMVEC sprouting after 48 hours revealed that the control fibrin gels failed to promote endothelial cell sprouting (Figure 3G). In contrast, fibrin gels containing FMOD stimulated HMVECs to form capillary sprouts, which invaded the gels and produced stable cord-

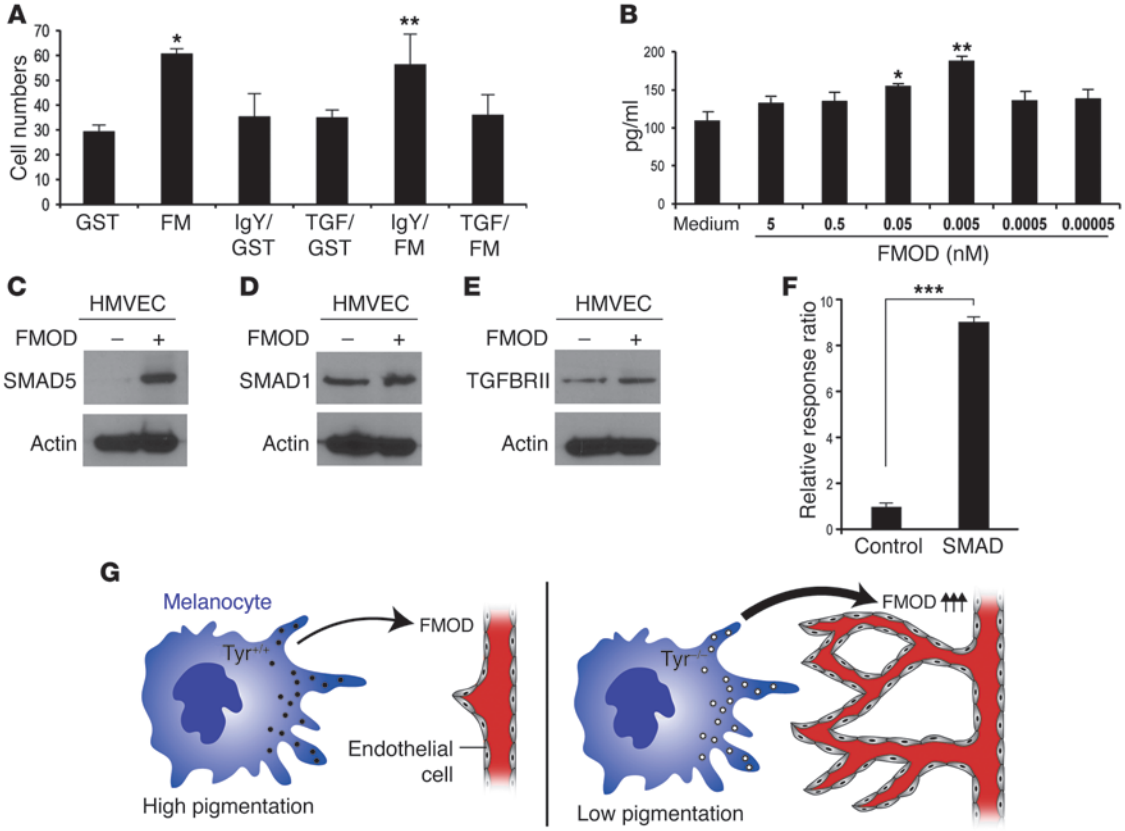

Figure 6

FMOD induces TGFB1 secretion by endothelial cells in vivo. (**A**) HMVECs treated with neutralized anti-TGFB1 overnight and HMVEC migration were assessed in response to 3 nM recombinant FMOD or control. $^{*}P = 0.00018$; $^{**}P = 0.002$. (**B**) FMOD at designated concentrations and time courses induces TGFB1 secretion, measured in pg/ml by ELISA. $P < 0.0001$. Experiment repeated more than 3 times. $^{*}P = 0.003$; $^{**}P = 0.0002$. (**C**–**E**) HMVECs treated with 0.5 nM FMOD were assessed by Western blot using antibodies against SMAD5 (**C**), SMAD1 (**D**), and TGFRII (**E**). β-Actin was used as a loading control. (**F**) HMVECs were transfected with SMAD reporter and negative and positive control and treated with recombinant FMOD or control. Dual luciferase assay was performed and values are expressed using Renilla for internal normalization. Experiments were done in triplicate and repeated at least 3 times. $^{***}P < 0.0001$. (**G**) Diagram showing the role of melanocytes in angiogenesis. Lower-pigmented melanocytes express higher levels of FMOD, which stimulates angiogenesis. All experiments were repeated 3 times and included 10 eyes per group in each experiment.

like structures (Figure 3G). This effect resembled the angiogenic response seen with a combination of FGF2 and VEGF-A in the positive control (Figure 3G). Detailed quantitative analysis by ANOVA revealed that 1.5 nM FMOD (75 sprouts) and positive control FGF2/VEGF-A combination (68 sprouts) produced similar numbers of capillary sprouts per bead (Figure 3H). However, FMOD stimulated the formation of significantly (57%) longer capillary structures (>150 μm) (Figure 3I). This FMOD-induced augmentation of capillary sprouting is consistent with its ability to form an extensive capillary network on 2D Matrigel (Supplemental Figure 4). Additionally, we conducted spheroid assays to provide enhanced imaging of the vasculature. This 3D in vitro assay simulates the proteolytic activity, migration and proliferation of the angiogenic process. HMVECS incubated for 24 hours in collagen type I with 4.5 nM recombinant FMOD had elevated outgrowth of sprouts when compared with those incubated in collagen alone (Supplemental Figure 5). Taken together, these in vitro assays demonstrate that FMOD is a potent stimulator capable of influencing pivotal steps in the angiogenic process, including endothelial cell proliferation, migration, sprouting, and capillary network formation.

FMOD stimulates angiogenesis in vivo. We next investigated the effect of FMOD on capillary formation in vivo. We utilized a model combining HMVECs with human bone marrow–derived mesenchymal stem cells (hBM-MSC), cells which support and stimulate angiogenesis (36). The cells were suspended in Matrigel and injected subcutaneously into the flanks of nude mice. Plugs were harvested after 7 days. To visualize the pattern of vessel formation and confirm their functional integration with the host vasculature, human-specific rhodamine-labeled lectin was injected intravenously and allowed to circulate for 15 minutes prior to harvesting the Matrigel plugs. The vascular plexus was visualized using laser confocal microscopy. Figure 4A shows that FMOD formed a robust functional capillary plexus with significantly more capillaries branching off larger vessels when compared with HMVEC+hBM-MSC alone.

To demonstrate whether neutralization of FMOD in vivo could correspondingly diminish the angiogenic effect of albino melanocytes, we performed a modified Matrigel assay. Nonpigmented melanocytes were mixed with Matrigel in the presence of anti-FMOD antibody or control IgG and injected subcutaneously.

After 6 days, Matrigel plugs were removed and invading mouse CD31-positive endothelial cells were quantified by FACS as previously described (ref. 37 and Figure 4B). Strikingly, we found that FMOD neutralization reduced the number of CD31-positive cells by 2.25-fold (Figure 4C), reinforcing the conclusion that FMOD is an angiogenic factor in amelanotic tissue. We next utilized the corneal micropocket angiogenesis assay to further highlight this role. Pellets containing either FMOD (1.7 pmol/pellet), GST (1.7 pmol/pellet, negative control), or VEGF-A (5.2 pmol/pellet, positive control) were implanted into the corneas of C57BL mice. Corneas were analyzed 5 days after implantation. FMOD pellets stimulated corneal neovascularization with a VA similar to that seen with 3 times higher amounts of VEGF-A (Figure 4D). Evaluation of vessel length showed that FMOD promoted formation of extensive vessel structures (Figure 4E), thus mirroring in vitro phenomena (Figure 3I). To investigate whether FMOD's activity is unique in its class, we performed negative control studies with lumican, an extracellular matrix protein which is also a member of the small leucine–rich proteoglycans (SLRP). Lumican has high homology to FMOD and binds as well to fibrillar collagens. Although it is known that lumican regulates collagen fibrillogenesis (28), our experiments showed it to have no effect on angiogenesis (Supplemental Figure 6). To determine whether FMOD enhances CNV formation, 4 subretinal laser burns were placed per eye in C57BL mice. On the day of laser induction, intravitreal injection of 35 ng/0.5 μl/eye rh-FMOD or GST (sham injection control) was performed. On day 14, the size of CNV lesions in all groups was measured. The FMOD-treated group was found to have increased CNV, 37.4% compared with the control group (Figure 5, A and B).

Continuing our in vivo studies, we then evaluated the proangiogenic effects of FMOD in wound repair, utilizing a cutaneous ear wounding model in C57BL mice. Ear wounds were treated topically with recombinant FMOD (2 μM) or control (GST) daily for 5 days. Neovascularization was evaluated on day 5 by injecting mice with FITC-conjugated dextran to highlight functional blood vessels (Figure 4F). Quantification of the fluorescent vessels surrounding the wound demonstrated that treatment with recombinant FMOD yielded a doubling of the mean fluorescent signal when compared with control. These data show that exogenous FMOD increases microvessel density in the wound-healing microenvironment (Figure 4G).

We next sought to investigate the potential role of FMOD in developmental angiogenesis. Mice were injected intravitreally with 0.5 μl of 1.19 μM recombinant FMOD or control GST on postnatal day 4. Analysis on day 7 revealed that in control mice, the retinal capillary plexus had expanded from the optic disc in a normal fashion (Figure 4H). However, mice treated with FMOD (Figure 4H) exhibited a 73% increase in microvessel density (Figure 4I) with a corresponding 27% decrease of avascular area in their retinas (Figure 4J).

FMOD-deficient mouse strains are currently only available as pigmented mice on the C57BL background. However, since the level of FMOD is already very low in pigmented melanocytes, lowering or blocking FMOD in these animals will not be useful in evaluating the role of melanocyte-secreted FMOD in angiogenic diseases. We believe this is the reason that previous studies with pigmented *Fmod*-KO mice have failed to expose dramatic differences, due to the inherently low levels of FMOD in black mice. We therefore bred $Fmod^{-/-}$ mice (a gift from A. Oldberg, Lund University, Lund, Sweden) onto an albino background ($Tyr^{-/-}$) to better examine the role of FMOD in angiogenesis in the absence of pigmentation. We first performed Matrigel angiogenesis assays in the skin of $Fmod^{+/+}$ (WT) or $Fmod^{-/-}$ (KO) mice in both black (C57) and white ($Tyr^{-/-}$) backgrounds. We found a dramatic reduction (71.5%) in the number of CD31-positive endothelial cells infiltrating the Matrigel in FMOD-deficient albino mice (Figure 5C) compared with control albino mice. Additionally, a similar reduction was found in the number of CD31-positive endothelial cells infiltrating into the Matrigel in black mice (C57BL) compared with white mice ($Tyr^{-/-}$ C57) (Figure 5C). As anticipated, we observed minimal differences between experimental angiogenesis elicited in black WT control mice versus black *Fmod*-KO mice.

In order to compare neovascularization arising in the iris, FGF2 pellets were implanted in the corneas of $Fmod^{+/+}$ or $Fmod^{-/-}$ (KOs) in both black (C57) and white ($Tyr^{-/-}$) mice. After 5 days, iris vessels and neovascularization were visualized via intravenous injection with FITC-conjugated BS-1 lectin to label perfused blood vessels. Analysis, performed using Angiotool software (38), revealed 2.4-fold greater VA in the iris of $Fmod^{+/+}$ albino mice (Figure 5D) when compared with $Fmod^{-/-}$ albino mice (Figure 5E). $Fmod^{-/-}$ mice had a 34% reduction in total vessel length versus WT (Figure 5F). We also measured vessel branching and found that it was reduced by 32% in *Fmod*-KO albino mice (Figure 5G).

To further investigate angiogenesis in the KO mice, we performed a pathophysiologic animal model of retinal vein occlusion (RVO) (39). In this model, iris neovascularization occurs following venous thrombosis, elicited by photocoagulating the vein close to the optic nerve using a laser. 50-μM burns were created with a power setting of 150 mW in white mice. After 14 days, iris vessels and neovascularization were visualized by Alexa Fluor 647 conjugated to lectin GS-II and analyzed by Angiotool software (Figure 5H). Measurement of the iris VA of $Fmod^{+/+}$ albino mice revealed a 40% decrease in iris vessels in $Fmod^{-/-}$ albino mice (Figure 5I). Further, total numbers of branches were reduced by 38% in *Fmod*-KO animals (Figure 5J).

FMOD stimulates TGFB1 secretion in vitro. To examine how FMOD stimulates endothelial cells, we investigated FMOD's known interaction with TGFB1 (40). We tested whether FMOD stimulates endothelial migration through the binding of TGFB1. To determine this, we incubated endothelial cells overnight with a TGFB1-neutralizing antibody. After 24 hours, those cells were subject to a standard migration assay as described previously, where cells were stimulated to migrate across an 8-μm Transwell in the presence of positive control, negative control, or FMOD. We observed that TGFB1 antibodies neutralized the promigratory effects of FMOD on HMVEC (Figure 6A). To study the molecular mechanism behind this observation, we utilized an in vitro culture and examined secretion levels of the active form of TGFB1 from the extracellular matrix of HMVECs in response to FMOD. After exposing HMVECs to designated concentrations of FMOD, we measured the active form of TGFB1 secreted after 2 hours and found a maximal increase with 0.005 nM of FMOD (Figure 6B).

TGFB signaling is mostly mediated via a receptor complex composed of TGFBRII and TGFBRI. TGFB1 signal, through a TGFBRII in association with activin receptor-like kinase 1 (ALK1), activated endothelial cells and resulted in elevated proliferation and migration (41, 42). This activates the canonical SMAD-dependent pathway via SMAD5 phosphorylation. We found that HMVECs that were incubated with 0.005 nM of FMOD for 30 minutes had increased levels of phosphorylated SMAD5, SMAD1, and TGFRII

(Figure 6, C–E). This in turn increased levels of SMAD5, SMAD1, and TGFBRII. In order to examine the signaling pathway regulated by SMAD, HMVECs were transduced with a SMAD reporter (lentivirus). After 24 hours, cells were treated with 0.5 nM FMOD overnight. Dual luciferase assay revealed that FMOD activated the SMAD reporter 82-fold over control (Figure 6F). We therefore conclude that FMOD's stimulatory effect on endothelial cells functions in part through its ability to bind to TGFB1 and mediate the SMAD-dependent pathway.

Discussion

Angiogenesis, the formation of new blood vessels, is regulated by cytokines and growth factors in a highly orchestrated manner. Based on epidemiological evidence of an association between pigmentation levels and propensity for angiogenic diseases, we hypothesized that melanocytes in the microenvironment contribute to local regulation of neovascularization. Through our experiments, we defined what we believe to be a novel mechanism in which melanocytes secrete a previously unknown angiogenic factor, FMOD (Figure 5I). We show that FMOD serves an angiogenic function in tissues containing melanocytes, such as the iris, choroid, and skin. FMOD appears to be a potent stimulator of multiple steps in the angiogenic process, including endothelial cell growth, migration, sprouting, and capillary network formation. Our data reveal that FMOD stimulated blood vessel formation and accelerated neovascularization in 5 independent in vivo models. Additionally, knocking down FMOD in 3 independent in vivo models reduced angiogenesis. Mechanistically, FMOD activates endothelial cells via TGFB1 secretion. This in turn stimulates TGFRII, initiating the SMAD pathway, and ultimately resulting in activation of SMAD transcription factor.

It was previously reported (43) that corneal neovascularization in black mice lacking FMOD is similar to that in black WT mice and that, developmentally, these KOs are viable and fertile (23). Furthermore, a tumor study conducted in black *Fmod*-KO mice did not report an influence of FMOD on tumor angiogenesis (44). In our own studies, we also observed minimal differences between experimental angiogenesis elicited in C57 black *Fmod*-KO mice versus black WT control mice. However, as our in vitro data has emphasized, the baseline levels of FMOD in pigmented melanocytes are very low compared with those in albino melanocytes. This suggests that Oldberg et al. failed to detect FMOD's effects on the angiogenic process because of the inherently low level of FMOD expression in both groups of their black animals. Therefore, we created albino *Fmod*-KO mice to evaluate differences in FMOD expression at levels where they can be observationally appreciated and experimentally manipulated. Our experiments reveal a dramatic reduction of angiogenesis in *Fmod*-KO albino mice compared with WT albinos. Regarding the viability of *Fmod*-KO mice, we note that there are many strains of mice that have genetic KOs of an angiogenic factor such as thrombospondin, neuropilin, semaphorin, and RhoB, that are both viable and fertile. Thus *Fmod*-KO mice may not exhibit a gross angiogenic phenotype during development because genetic redundancy often preserves physiological angiogenesis.

In conclusion, we provide genetic and biochemical data that elucidate the epidemiological correlation between pigmentation and susceptibility to angiogenic disease. Our findings suggest FMOD could be a promising therapeutic target for treating pathological angiogenesis, with the potential to ameliorate disease processes affecting pigmented tissues, such as in AMD, melanomas, and hemangiomas.

Methods

Materials. Rabbit anti-human FMOD monoclonal antibody was obtained from Sigma-Aldrich for immunoblotting; antibody for immunohistochemistry was obtained from Axxora and Proteintech Group Inc. Goat anti-mouse CD31 polyclonal antibody was obtained from R&D Systems, rabbit anti-human vWF was obtained from Dako, and rabbit anti-human TGFRI, SMAD2, and SMAD4 were from Cell Signaling. Several recombinant FMOD proteins from OriGene, Proteintech Group Inc., and Novus Biologicals were tested. Recombinant hVEGF-A and h-FGF2 were purchased from R&D Systems. For FMOD knockdown, we used SMARTpool siRNA from Dharmacon Inc. TGFB1 ELISA was purchased from R&D Systems.

Mice. C57 mice and B6(Cg)-*Tyr*$^{c\text{-}2J}$/J (C57-albino) mice (8 weeks old) were purchased from Jackson Laboratories. B6 (Cg)-*Tyr*$^{c\text{-}2J}$/J mice have a G-to-T base change at nucleotide 291 in the Tyrosinase gene. FMOD-deficient mice on a C57 background were a gift from Ake Oldberg. FMOD-deficient mice were bred to B6 (Cg)-*Tyr*$^{c\text{-}2J}$/J mice at the animal research facility at Boston Children's Hospital.

Cell culture. HMVEC-d (where d indicates *dermal*) cells and human melanocytes were obtained from ScienCell Research Laboratories. Other HMVECs were from Invitrogen and were grown according to the manufacturer's protocol. Each lot of human melanocytes consisted of cells from a single donor. We used 1 lot for each repetition; therefore, our data represent 10 donors (5 mixed European descent, 5 African-American) across our experiments.

Cells were plated on tissue culture dishes for molecular biochemical assays and on attachment-coated glass coverslips for cell staining. Mouse melanocytes were a gift from Alexeev Y. Vitali.

Choroidal melanocytes were derived from choroidal tissue of C57BL and C57-albino mice. Cells were collected by scrubbing the tissue, and were then established in RPMI medium containing 10% FCS and β-mercaptoethanol (βME; 55 mM). The growth medium was replaced 2 days after the initial seeding, every 2 to 3 days for at least 14 days, and then analyzed.

Biochemical methods. Irises or choroidal cells were isolated from C57BL and C57-albino mice and analyzed by Western blot. Nonpigmented melanocytes transfected with siRNA to silence FMOD were lysed and total protein quantified. 40 μg samples were loaded on 4%–12% PAGE gel, blotted, and incubated with rabbit anti–h-vWF, rabbit anti–h-FMOD, rabbit anti–h-FMOD, anti–TGF-β1, anti–TGFRII, anti-SMAD1, anti-SMAD5, and β actin–HRP. Pierce (GE Healthcare) detection reagents were used to visualize HRP-labeled secondary antibodies. Quantitative PCR (qPCR) was performed with Quantitect TaqMan (Applied Biosystems) using the Mx3005P QPCR System (Agilent Technologies); FMOD or GAPDH (control) primers were obtained from Applied Biosystem.

CM. Equal numbers of nonpigmented or pigmented melanocytes were plated on tissue culture plates overnight. A day later, the medium was replaced using HMVEC-d medium. After 24 to 48 hours, CM was collected and the cells were counted again. The amount of CM was calculated relative to 10^6 cells/ml.

Cell proliferation assay. HMVEC-d cells were plated at 10,000 cells/ml onto 24-well culture plates in EGM medium with supplements and challenged with recombinant FMOD (4.6 nM, 1.5 nM, and 0.5 nM) or with CM from melanocytes. Cells were then trypsinized, and cell counts were recorded using a TC10 automated cell counter (Bio-Rad). WST-1 was used to assess viable cells (Roche). Colorimetric absorbance of the samples was read at 420–480 nm. Experiments were repeated at least 3 times.

Cell migration assay. Cell migration was performed as previously described (45) with the following modifications: HMVEC-d were seeded (10^5 cells/100 μl) onto the upper chamber and allowed to migrate toward CM from melanocytes or that containing recombinant protein present in the bottom of the well. Then cells were stained with Giemsa and counted in

10 random fields (×400). Migrated cells were detached, lysed, labeled with a fluorescent dye, and measured with a fluorescence microplate reader (PerkinElmer). Experiments were repeated at least 3 times.

Transcription factor assay. The HMVECs were cultured for 24 hours and then infected with pCignal Lenti TRE reporter gene (Smad) or control reporter for an additional 48 hours to ensure lentivirus integration (SAbioscience; QIAGEN). The cultures were then treated with 2 nM recombinant FMOD overnight. Promoter activity was measured after Dual-Glu luciferase reagent (Promega) was added to the cultured cells. We measured the firefly luminescence by the laminator (Vector3), and results were calculated as relative response ratio (RRR): (experimental sample ratio) – (negative control ratio)/(positive control ratio) – (negative control ratio).

In vitro 3D sprouting assay. HMVEC-d was cultured on Cytodex-3 microcarrier beads (Amersham Biosciences) coated with fibrinogen at a density of 200 cells per bead. Cells and beads were suspended in 5 ml endothelial basal medium (EBM) mixed gently every hour for the first 4 hours. The mixture was then cultured overnight at 37°C. The next day, hMVEC-d bead culture was embedded in 1 mg/ml fibrin gel with EBM with or without recombinant FMOD (1.5 nM or 4.6 nM) in a 48-well plate for 2 days. A combination of angiogenic factors, FGF2 (1.5 nM), and VEGF-A (1.5 nM) was used as the positive angiogenic control. The effect of the angiogenic factors on sprout angiogenesis was quantified visually by determining the number and percentage of HMVEC beads with capillary sprouts.

In vivo angiogenesis assays. Matrigel plugs with nonpigmented melanocytes mixed with rabbit anti-FMOD or control rabbit IgG were implanted subcutaneously on the backs of C57BL/6 mice. After 6 days, plugs were enzymatically digested and FACs analysis was performed. Quantification of endothelial cells was defined as $CD31^+CD45^-$. Flow cytometry was performed using FACSCalibur and CellQuest software (BD Biosciences). HMVECs (1×10^6 cells/ml) were combined with hBM-MSC (0.1×10^6 cells/ml) at a ratio of 10:1 with or without FMOD (15 nM) and suspended in phenol red–free reduced Matrigel (final cell density = 5×10^6 cells/ml). This was injected subcutaneously into each flank of 6- to 8-week-old nude mice. After 7 days, 100 μl rhodamine-labeled lectin (Vector Labs) was injected intravenously and allowed to circulate for 15 minutes prior to harvesting the Matrigel implants. The harvested plugs were fixed with 4% paraformaldehyde overnight, and high resolution whole-mount imaging of the 3D vascular plexus was performed by using a Leica DMIRE2 laser confocal microscope.

Corneal micropocket assay. The corneal micropocket angiogenesis assay was performed as previously described (46). Pellets containing 80 ng carrier-free recombinant human FGF2, 50 ng VEGF-A (R&D Systems), 25 ng FMOD, or GST (as a control) were implanted into the corneas of C57BL or C57-albino mice. Five days later, vessel growth was measured. The area of neovascularization was calculated as follows: VA (mm^2) = (π × clock hour × vessel length [mm] × 0.2 mm). The experiments were repeated 3 times and included 10 eyes per group in each experiment.

Iris whole mounts. Following micropocket assay with FGF2 pellets (5× C57BL mice each per group), animals were injected with Lectin BS-1 FITC (Sigma-Aldrich). Mice were then sacrificed; eyes were removed and placed in formalin for 1 hour. Irises were then dissected, washed in PBS, and flat mounted on glass slides. Conventional fluorescent microscopy was used to capture images. Quantification of vessel density was performed with ImageJ (http://rsbweb.nih.gov/ij/).

Retina whole mounts. FMOD or control GST (0.833 nM/0.5 μl) was injected into the vitreous of 4-day-old C57BL mice. On day 7, animals were sacrificed and retinas were dissected and incubated with Lectin BS-1 TRITC (Sigma-Aldrich) overnight at 4°C. Flat mount was visualized and images captured by conventional fluorescent microscopy. Quantification of vessel density was performed with ImageJ. The experiments were repeated 3 times with 7 to 9 mice per group.

Wound healing. The dorsal aspect of the ear of C57BL and C57-albino mice was wounded with a circular 1-mm diameter punch. Wound neovascularization was assessed 5 days after wounding by injection of dextran-FITC. To test the effect of FMOD on this angiogenesis model, C57BL mice were wounded with a circular punch of 1 mm and treated daily with reduced growth factor Matrigel containing either recombinant FMOD or recombinant GST. Five days after wounding, mice were injected with dextran-FITC to visualize neovascularization. Pictures were taken with a Nikon Eclipse TE-2000-E fluorescence microscope using a Coolsnap HQ CCD camera. Quantification of newly built vessels was performed using ImageJ.

CNV model. C57 mice were anesthetized with avertin (400 mg/kg). The pupils were dilated with a mixture of 0.5% tropicamide and 0.5% phenylephrine hydrochloride (Santen Pharmaceutical). Lesions were induced by laser (power 150 mW) around the optic nerve through a slit lamp delivery system using a Nidek photocoagulator (GYC2000; Nidek). Four burns were performed per eye around the optic disc. 35 ng/0.5 μl/eye rh-FMOD or GST treatments were injected intravitreally at the day of CNV induction (day 0), and the sizes of CNV lesions were determined after 14 days. Fourteen days after laser induction, mice were euthanized and their eyes were removed and fixed in 4% paraformaldehyde for 60 minutes. The choroids were carefully dissected from the eyecup. Blood vessels were labeled using a 1:200 dilution of isolectin IB4 (Vector Laboratories). Fluorescent images of choroidal flat mounts were captured using a CCD camera (DC500; Leica). The CNV areas, presented in μm^2, were evaluated using Scion image software.

RVO model. Mice were anesthetized with avertin (400 mg/kg) as described in the CNV model. The pupils were dilated with a mixture of 0.5% tropicamide and 0.5% phenylephrine hydrochloride (Santen Pharmaceutical). Venous points were selected close to the optic nerve through a slit lamp delivery system using a Nidek photocoagulator (GYC2000; Nidek). A power setting of 50 mW for C57 mice and 150 mW for C57-albino mice was applied for a duration of 3 seconds to create a spot size of 50 μm. Five applications were conducted in order to stop blood flow. At 14 days after laser induction, mice were euthanized and their eyes were removed and fixed in 4% paraformaldehyde overnight (39). The irises were carefully dissected and blood vessels were labeled using a 1:200 dilution of Lectin GSII (Molecular Probes). The fluorescent images of iris flat mounts were captured using a CCD camera (DC500; Leica). The areas of neovascularization (presented in μm^2) were evaluated using Scion image software.

Skin immunofluorescence. 20-micron sections of OCT-frozen ears were fixed with acetone and labeled with rat anti-mouse CD31–FITC (BD Biosciences).

Microarray. Microarray data have been deposited in the GEO database (GSE51073).

Statistics. Data are expressed as mean ± SD. Statistical significance was assessed using Student's unpaired 2-tailed *t* test with Bonferroni correction, as appropriate, or ANOVA. $P < 0.05$ was considered statistically significant.

Study approval. All animal studies were reviewed and approved by the Institutional Animal Care and Use Committee of Boston Children's Hospital.

Acknowledgments

We acknowledge Ake Oldberg for generously sharing *Fmod*-KO mice. We also thank Alexeev Y. Vitali for murine melanocyte cells. This study was supported in part by a grant from the NIH (R01EY012726).

Address correspondence to: Irit Adini, Vascular Biology Program, Department of Surgery, Boston Children's Hospital, Harvard Medical School, 300 Longwood Avenue, Boston, Massachussetts 02115, USA. Phone: 617.919.2256; Fax: 617.730.0002; E-mail: irit.adini@childrens.harvard.edu.

1. Congdon N, et al. Causes and prevalence of visual impairment among adults in the United States. *Arch Ophthalmol*. 2004;122(4):477–485.
2. Gottlieb JL. Age-related macular degeneration. *JAMA*. 2002;288(18):2233–2236.
3. Vanderbeek BL, Zacks DN, Talwar N, Nan B, Musch DC, Stein JD. Racial differences in age-related macular degeneration rates in the United States: a longitudinal analysis of a managed care network. *Am J Ophthalmol*. 2011;152(2):273–282.e3.
4. Abdel-Malek Z, et al. Mitogenic and melanogenic stimulation of normal human melanocytes by melanotropic peptides. *Proc Natl Acad Sci U S A*. 1995; 92(5):1789–1793.
5. Hu DN, Yu GP, McCormick SA, Schneider S, Finger PT. Population-based incidence of uveal melanoma in various races and ethnic groups. *Am J Ophthalmol*. 2005;140(4):612–617.
6. Weis E, Shah CP, Lajous M, Shields JA, Shields CL. The association between host susceptibility factors and uveal melanoma: a meta-analysis. *Arch Ophthalmol*. 2006;124(1):54–60.
7. Costin GE, Hearing VJ. Human skin pigmentation: melanocytes modulate skin color in response to stress. *FASEB J*. 2007;21(4):976–994.
8. Sarangarajan R, Apte SP. Melanization and phagocytosis: implications for age related macular degeneration. *Mol Vis*. 2005;11:482–490.
9. Abdel-Malek Z, Swope V, Smalara D, Babcock G, Dawes S, Nordlund J. Analysis of the UV-induced melanogenesis and growth arrest of human melanocytes. *Pigment Cell Res*. 1994;7(5):326–332.
10. Fedorow H, Tribl F, Halliday G, Gerlach M, Riederer P, Double KL. Neuromelanin in human dopamine neurons: comparison with peripheral melanins and relevance to Parkinson's disease. *Prog Neurobiol*. 2005;75(2):109–124.
11. Galibert MD, Carreira S, Goding CR. The Usf-1 transcription factor is a novel target for the stress-responsive p38 kinase and mediates UV-induced Tyrosinase expression. *EMBO J*. 2001;20(17):5022–5031.
12. Hornyak TJ, Hayes DJ, Ziff EB. Cell-density-dependent regulation of expression and glycosylation of dopachrome tautomerase/tyrosinase-related protein-2. *J Invest Dermatol*. 2000;115(1):106–112.
13. Kobayashi T, et al. Tyrosinase related protein 1 (TRP1) functions as a DHICA oxidase in melanin biosynthesis. *EMBO J*. 1994;13(24):5818–5825.
14. Benedito E, et al. Melanin formation in the inner ear is catalyzed by a new tyrosine hydroxylase kinetically and structurally different from tyrosinase. *Biochim Biophys Acta*. 1997;1336(1):59–72.
15. Englaro W, et al. Inhibition of the mitogen-activated protein kinase pathway triggers B16 melanoma cell differentiation. *J Biol Chem*. 1998;273(16):9966–9970.
16. Winder A, et al. The tyrosinase gene family — interactions of melanogenic proteins to regulate melanogenesis. *Cell Mol Biol Res*. 1994;40(7–8):613–626.
17. Yokoyama K, Suzuki H, Yasumoto K, Tomita Y, Shibahara S. Molecular cloning and functional analysis of a cDNA coding for human DOPAchrome tautomerase/tyrosinase-related protein-2. *Biochim Biophys Acta*. 1994;1217(3):317–321.
18. Rohan RM, Fernandez A, Udagawa T, Yuan J, D'Amato RJ. Genetic heterogeneity of angiogenesis in mice. *FASEB J*. 2000;14(7):871–876.
19. Folkman J, Haudenschild CC, Zetter BR. Long-term culture of capillary endothelial cells. *Proc Natl Acad Sci U S A*. 1979;76(10):5217–5221.
20. Alexeev V, Yoon K. Stable and inheritable changes in genotype and phenotype of albino melanocytes induced by an RNA-DNA oligonucleotide. *Nat Biotechnol*. 1998;16(13):1343–1346.
21. Hedbom E, Heinegard D. Interaction of a 59-kDa connective tissue matrix protein with collagen I and collagen II. *J Biol Chem*. 1989;264(12):6898–6905.
22. Oldberg A, Antonsson P, Lindblom K, Heinegard D. A collagen-binding 59-kd protein (fibromodulin) is structurally related to the small interstitial proteoglycans PG-S1 and PG-S2 (decorin). *EMBO J*. 1989;8(9):2601–2604.
23. Svensson L, Narlid I, Oldberg A. Fibromodulin and lumican bind to the same region on collagen type I fibrils. *FEBS Lett*. 2000;470(2):178–182.
24. Sjoberg AP, et al. The factor H variant associated with age-related macular degeneration (His-384) and the non-disease-associated form bind differentially to C-reactive protein, fibromodulin, DNA, and necrotic cells. *J Biol Chem*. 2007;282(15):10894–10900.
25. Ameye L, Aria D, Jepsen K, Oldberg A, Xu T, Young MF. Abnormal collagen fibrils in tendons of biglycan/fibromodulin-deficient mice lead to gait impairment, ectopic ossification, and osteoarthritis. *FASEB J*. 2002;16(7):673–680.
26. Ameye L, Young MF. Mice deficient in small leucine-rich proteoglycans: novel in vivo models for osteoporosis, osteoarthritis, Ehlers-Danlos syndrome, muscular dystrophy, and corneal diseases. *Glycobiology*. 2002;12(9):107R–116R.
27. Antonsson P, Heinegard D, Oldberg A. Posttranslational modifications of fibromodulin. *J Biol Chem*. 1991;266(25):16859–16861.
28. Chakravarti S. Functions of lumican and fibromodulin: lessons from knockout mice. *Glycoconj J*. 2002;19(4–5):287–293.
29. Ezura Y, Chakravarti S, Oldberg A, Chervoneva I, Birk DE. Differential expression of lumican and fibromodulin regulate collagen fibrillogenesis in developing mouse tendons. *J Cell Biol*. 2000; 151(4):779–788.
30. Gori F, Schipani E, Demay MB. Fibromodulin is expressed by both chondrocytes and osteoblasts during fetal bone development. *J Cell Biochem*. 2001; 82(1):46–57.
31. Hedlund H, Mengarelli-Widholm S, Heinegard D, Reinholt FP, Svensson O. Fibromodulin distribution and association with collagen. *Matrix Biol*. 1994; 14(3):227–232.
32. Skerka C, et al. Defective complement control of factor H (Y402H) and FHL-1 in age-related macular degeneration. *Mol Immunol*. 2007;44(13):3398–3406.
33. Prota G. Regulatory mechanisms of melanogenesis: beyond the tyrosinase concept. *J Invest Dermatol*. 1993;100(2 suppl):156S–161S.
34. Hata Y, Rook SL, Aiello LP. Basic fibroblast growth factor induces expression of VEGF receptor KDR through a protein kinase C and p44/p42 mitogen-activated protein kinase-dependent pathway. *Diabetes*. 1999;48(5):1145–1155.
35. Ley CD, Olsen MW, Lund EL, Kristjansen PE. Angiogenic synergy of bFGF and VEGF is antagonized by Angiopoietin-2 in a modified in vivo Matrigel assay. *Microvasc Res*. 2004;68(3):161–168.
36. Melero-Martin JM, et al. Engineering robust and functional vascular networks in vivo with human adult and cord blood-derived progenitor cells. *Circ Res*. 2008;103(2):194–202.
37. Adini A, Fainaru O, Udagawa T, Connor KM, Folkman J, D'Amato RJ. Matrigel cytometry: a novel method for quantifying angiogenesis in vivo. *J Immunol Methods*. 2009;342(1–2):78–81.
38. Zudaire E, Gambardella L, Kurcz C, Vermeren S. A computational tool for quantitative analysis of vascular networks. *PLoS One*. 2011;6(11):e27385.
39. Zhang H, Sonoda KH, Qiao H, Oshima T, Hisatomi T, Ishibashi T. Development of a new mouse model of branch retinal vein occlusion and retinal neovascularization. *Jpn J Ophthalmol*. 2007;51(4):251–257.
40. Soo C, et al. Differential expression of fibromodulin, a transforming growth factor-beta modulator, in fetal skin development and scarless repair. *Am J Pathol*. 2000;157(2):423–433.
41. Oh SP, et al. Activin receptor-like kinase 1 modulates transforming growth factor-beta 1 signaling in the regulation of angiogenesis. *Proc Natl Acad Sci U S A*. 2000;97(6):2626–2631.
42. Shao ES, Lin L, Yao Y, Bostrom KI. Expression of vascular endothelial growth factor is coordinately regulated by the activin-like kinase receptors 1 and 5 in endothelial cells. *Blood*. 2009; 114(10):2197–2206.
43. Schonherr E, et al. Decorin deficiency leads to impaired angiogenesis in injured mouse cornea. *J Vasc Res*. 2004;41(6):499–508.
44. Oldberg A, et al. Collagen-binding proteoglycan fibromodulin can determine stroma matrix structure and fluid balance in experimental cancinoma. *Proc Natl Acad Sci U S A*. 2007;104(35):13966–13971.
45. Satchi-Fainaro R, et al. Inhibition of vessel permeability by TNP-470 and its polymer conjugate, caplostatin. *Cancer Cell*. 2005;7(3):251–261.
46. Rogers MS, Birsner AE, D'Amato RJ. The mouse cornea micropocket angiogenesis assay. *Nat Protoc*. 2007;2(10):2545–2550.